Journal of Physics:
Condensed Matter

Thermodynamics and entropic inference of nanoscale magnetic structures in Gd

OPEN ACCESS
IOP Publishing
Journal of Physics: Condensed Matter
J. Phys.: Condens. Matter **37** (2025) 065705 (11pp)
https://doi.org/10.1088/1361-648X/ad92ee

Thermodynamics and entropic inference of nanoscale magnetic structures in Gd

Christian Binek[1,*], **Syed Qamar Abbas Shah**[1] **and Balamurugan Balasubramanian**[2]

[1] Department of Physics & Astronomy and the Nebraska Center for Materials and Nanoscience, University of Nebraska-Lincoln, Lincoln, NE 68588-0299, United States of America
[2] GKN Hoeganaes, Cinnaminson, NJ 08077, United States of America

E-mail: cbinek@unl.edu

Received 3 September 2024, revised 4 November 2024
Accepted for publication 14 November 2024
Published 26 November 2024

Abstract

A bulk gadolinium (Gd) single crystal exhibits virtually zero remnant magnetization, a common trait among soft uniaxial ferromagnets. This characteristic is reflected in our magnetometry data showing virtually hysteresis free isothermal magnetization loops with large saturation magnetization. The absence of hysteresis allows to model the measured easy axis magnetization as a function of temperature and applied magnetic field, rather than a relation, which permits the application of Maxwell relations from equilibrium thermodynamics. Demagnetization effects broaden the isothermal first-order transition from negative to positive magnetization. By analyzing magnetization data within the coexistence regime, we deduce the isothermal entropy change and the field-induced heat capacity change. Comparing the numerically inferred heat capacity with relaxation calorimetric data confirms the applicability of the Maxwell relation. Analysis of the entropy in the mixed phase region suggests the presence of hitherto unresolved nanoscale magnetic structures in the demagnetized state of Gd. To support this prediction, Monte Carlo simulations of a 3D Ising model with dipolar interactions are performed. Analyzing the cluster size statistics and magnetization from the model provides strong qualitative support of our analytic approach.

Keywords: entropy, domains, gadolinium, magnetocaloric, Monte Carlo, heat capacity, magnetometry

1. Introduction

Gadolinium (Gd) is a magnetically soft, archetypical magnetocaloric material often used as reference standard for magnetocaloric applications in near room temperature refrigeration [1–5]. Its superb magnetocaloric properties originate from the near room temperature critical temperature, $T_C = 292$ K, and its large atomic moment comprising a 7 μ_B contribution from localized 4f electrons and a 0.55 μ_B contribution from itinerant 5d valence electrons. Notably, experiments with ultrashort optical excitation show that these two contributions have distinctly different dynamic responses[6]. However, this intriguing effect can be disregarded in the context of static magnetometry and calorimetry. Magnetic and caloric properties of Gd have been intensely studied [1, 7–9]. Investigations into fundamental magnetic properties involve density functional theory (DFT) calculations to analyze ground state properties, such as the magnetic moment, by applying and comparing both the local density approximation

* Author to whom any correspondence should be addressed.

and the generalized gradient approximation for the exchange-correlation functional [10]. Frietsch *et al* employed DFT to calculate the intra- and inter-atomic exchange energies, which were used as input parameters for numerically solving the stochastic Landau–Lifshitz–Gilbert equation revealing the temperature dependence of the magnetization contributions from the 4f and 5d spins [6]. However, it is important to note that this approach does not account for the effects of dipolar interaction, which are investigated in our work. Fundamental questions regarding the magnetism of Gd, including the exact nature of its magnetic ordering remain under debate [11].

In this study, we examine the isothermal entropy change in the demagnetization-broadened regime of coexisting up and down magnetization and explore its implications for heat capacity and magnetic domain structure. While the entropy change in Gd has been extensively studied at temperatures near and above T_C [12], the entropy change occurring at the isothermal first-order transition at temperatures $T < T_C$ has received little attention. This contrasts with the well-studied entropy changes at temperature-driven first-order transitions in materials such as metamagnets and Heusler shape-memory alloys [13, 14].

There are a number of reasons for limited interest in isothermal first order transitions in the context of magnetocaloric phenomena. Firstly, the entropy change and adiabatic temperature change are generally small away from T_C. That holds for the paramagnetic phase but is especially true in the long range ordered phase. Additionally, in many magnetic materials, long-range order is accompanied by magnetic hysteresis, which is detrimental to magnetocaloric performance [15]. Second, when guided by an oversimplified theoretical picture, where dipolar interaction between magnetic moments is neglected and the isothermal first order transition is strictly discontinuous, the Clapeyron relation suggests absence of isothermal entropy change. This occurs because, in a first-order transition, the entropy change is proportional to the slope of the phase transition line. The description of isothermal magnetization reversal in terms of a first order phase transition is well established in the literature [16]. For a ferromagnet, the phase transition line is given by $H(T < T_C) = 0$, which implies that $\mathrm{d}H/\mathrm{d}T = 0$. However, in real samples, where the applied magnetic field, H_a, and the internal magnetic field, H, differ by the demagnetizing field, the first order transition is broadened. In the absence of hysteresis, the magnetization, M, becomes a continuous function of H_a. There are quasi equilibrium magnetization states in the vicinity of $M(H_a = 0, T < T_C)$ which do not exist in the absence of demagnetizing effects where M is discontinuous at $H = 0$.

In soft uniaxial ferromagnets such as Gd, $M(H_a = 0, T < T_C) = 0$ implies the presence of a fully demagnetized multi-domain state entailing a highly inhomogeneous internal magnetic field, H. As a result, there is no individual value H, other than the theoretical construct of the spatial average, which can be associated with a given value of the applied homogeneous field H_a. In this situation, which is more common than exceptional, the concept of a purely geometry-dependent demagnetizing tensor or demagnetizing factor does not apply [17]. When attempting to artificially associate H_a with a field $H = H_a - D_{eff}M$, the effective demagnetizing factor, D_{eff}, becomes weakly temperature dependent. The T-dependence indicates the breakdown of the concept of a homogeneous demagnetizing field which requires $\nabla \underline{M} = 0$, a condition clearly violated in a multi-domain state. When ignoring the inapplicability of the concept of a geometry dependent demagnetizing factor and plotting M versus $H = H_a - D_{eff}M$ with $D_{eff} = 1/\frac{\partial M}{\partial H_a} \approx \text{const}$, the resulting M versus H curve displays, per construction, a discontinuous step ΔM at $H = 0$ reminiscent of a theoretical model with negligible dipolar interaction. Although this procedure is often used in the literature to compare theoretical and experimental results, it is, strictly speaking, based on prerequisites which are not fulfilled. The appropriate representation of experimental data in the generic case of inhomogeneous magnetization is M versus H_a as measured without data manipulation motivated by an idealized theory that does not include dipolar interaction and geometry of finite samples [18]. In this work we investigate the little explored thermal and magnetic properties within the mixed phase region of the demagnetization broadened first order isothermal transition of a Gd single crystal.

2. Experimental results, modeling, simulation and discussion

2.1 Magnetometry

Figure 1 displays M versus H_a data measured via integral superconducting quantum interference device (SQUID) magnetometry (Quantum Design MPMS) at temperatures of $T = 280$ K (red squares connected by lines) and $T = 290$ K (blue line). These measurements were conducted on a cylindrical sample with a mass of 4.87 mg, with H_a applied along the cylinder axis collinear to the crystal's *c*-axis. The upper left inset of figure 1 shows M vs H for both temperatures (same color coding), where $H = H_a - D_{eff}M(H_a, T)$. The respective D_{eff} was determined as $D_{eff} = 1/(\partial M/\partial H_a)_T$ from the reciprocal slopes of linear best fits in the field regime $-0.04 < H_A < 0.04$ MA m^{-1}, i.e. within the region of phase coexistence. There is a small but significant difference (about 5%) between $D_{eff}(T = 280\ \mathrm{K}) = 0.323$ and $D_{eff}(T = 290\ \mathrm{K}) = 0.333$. A systematic investigation of the temperature dependence of D_{eff} is shown in the lower right inset of figure 1 where D_{eff} has been numerically calculated from a set of M versus T data taken at various applied magnetic fields $7.4 \leq H_a \leq 126.7$ kA m^{-1}. Those M versus T data are shown in figure 2 (right panel) together with the $T = 280$ K isothermal cut creating the M vs H_a data shown as open circles in the left panel. Those circles fall virtually perfectly on the data shown as squares (figure 2 left panel) from the measurement of the M vs H_a isotherm. Arrows between the right and left panel of figure 2 visualize the mapping between M vs T and M vs H_a data.

2.2. Modeling the equation of state from magnetization data

The isothermal entropy change and the change in heat capacity with applied magnetic field can be determined from

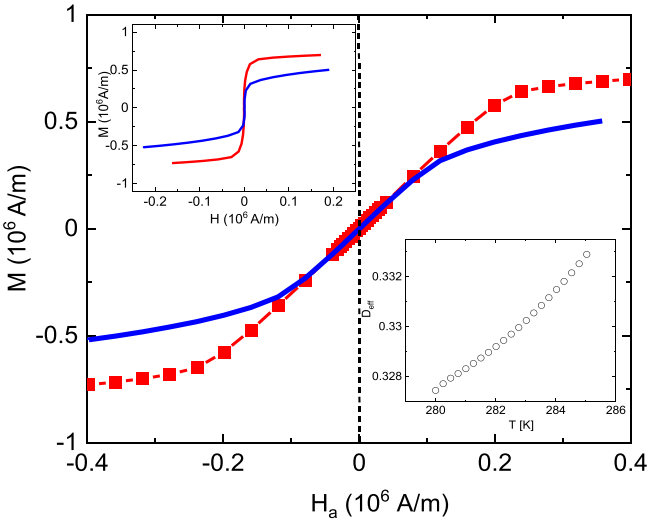

Figure 1. M versus H_a data at $T = 280$ K (red squares connected by lines) and $T = 290$ K (blue line). Upper left inset shows M vs H with $H = H_a - D_{\rm eff}M(H_a, T)$ and $D_{\rm eff}(T = 280\ {\rm K}) = 0.323$ and $D_{\rm eff}(T = 290\ {\rm K}) = 0.333$. Lower right inset shows systematic investigation of the temperature dependence of $D_{\rm eff}$ with $D_{\rm eff}$ numerically calculated from M versus T data taken at various applied magnetic fields $7.4 \leq H_a \leq 126.7$ kA m^{-1}.

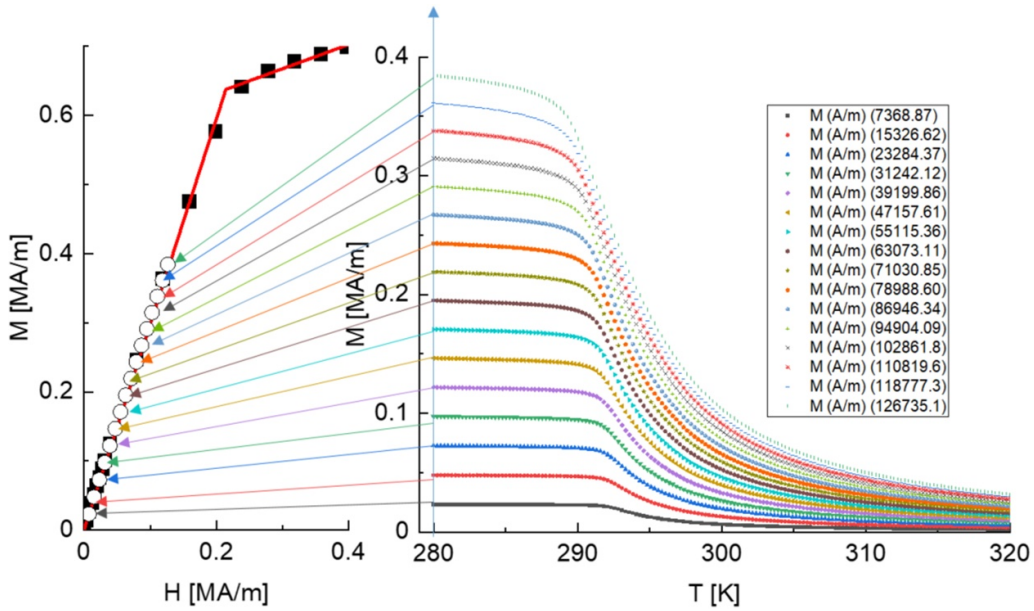

Figure 2. (Right panel) M vs T for applied magnetic fields $7.4 \leq H_a \leq 126.7$ kA m^{-1}. Vertical arrow represents the isothermal cut through the data set at $T = 280$ K creating the M vs H_a data shown as open circles in the left panel. Arrows between right and left panel visualize the mapping between M vs T and M vs H_a data. (Left panel) shows M vs H_a (solid squares) from isothermal SQUID measurement. The solid line resembles a best fit of a phenomenological model function.

magnetization data by integrating the Maxwell relation associated with the analytical behavior of the Gibbs free energy [18]. The heat capacity change depends on the temperature derivative of the entropy change and thus involves $\left(\frac{\partial^2 M}{\partial T^2}\right)_{H_a}$. Numerical calculation of higher order derivatives from experimental data is often hampered by noise. To address this issue, we design a phenomenological functional form of the equation of state $M(H_a, T)$ which summarizes all field and temperature dependent measured data and allows to calculate derivatives of the magnetization without accumulation of noise. For simplicity, but without loss of generality, we begin modeling $M(H_a, T)$ by looking at the first quadrant of M vs H_a.

In the regime of coexisting up and down magnetization, $H_a < H_c(T)$, we express the integral magnetization of the Gd sample as

$$M(H_a, T) = \chi(T) H_a + \left(M_\uparrow(T) \frac{V_\uparrow(H_a)}{V} + M_\downarrow(T) \frac{V_\downarrow(H_a)}{V} \right). \quad (1)$$

Here $H_c(T)$ is the magnetic field strength above which the sample is in a magnetic single domain state, $\chi(T)$ is a temperature dependent effective local linear magnetic susceptibility, which is the same for up (↑) and down (↓) magnetized regions, $M_{\uparrow,\downarrow}(T)$ is the temperature dependent up/down spontaneous magnetization with $M_\uparrow = -M_\downarrow$ and $V_{\uparrow,\downarrow}$ is the up/down magnetized volume of the sample of total volume $V = V_\uparrow + V_\downarrow$. Because the magnetization isotherms (see figure 1) show in very good approximation a linear H_a-dependence for $H_a < H_c(T)$ one can conclude that the volume fractions $V_{\uparrow,\downarrow}/V$ are linear functions of H_a according to $V_{\uparrow,\downarrow}/\mathrm{V} = \frac{1}{2}\left(1 \pm \frac{H_a}{H_c}\right)$. Substituting this result into equation (1) yields

$$M(H_a,T) = \chi(T)H_a + M_\uparrow \frac{H_a}{H_c}. \quad (2)$$

For $H_a > H_c(T)$, i.e. outside the coexistence regime when the sample is uniformly up magnetized such that $V_\uparrow = V$, we obtain $M(H_a,T) = \chi(T)H_a + M_\uparrow$. Combining this result with equation (2) yields the empirical equation of state at temperatures below T_C and above the spin reorientation temperature $T_{SR} = 230$ K. T_{SR} is the temperature below which the magnetic easy axis starts to deviates from the [0001] direction of the hexagonal lattice [1, 19]. We restrict our investigation to temperatures $T > T_{SR}$. The final functional form of the equation of state reads

$$M(H_a,T) = \begin{cases} \chi(T)H_a + M_\uparrow(T)\frac{H_a}{H_c(T)} for H_a < H_C(T) \\ \chi(T)H_a + M_\uparrow(T) for H_a > H_c(T) \end{cases}. \quad (3)$$

Figure 3 shows, for the example of the $T = 280$ K magnetization isotherm, how the experimental data provide the parameters entering equation (3).

The critical field $H_c(T = 280\ \mathrm{K})$ marks the transition from the phase coexistence regime of high slope, $\frac{\partial M}{\partial H_a} = \chi + \frac{M_\uparrow}{H_c}$, to the single domain regime with slope χ. The spontaneous magnetization $M_\uparrow(T = 280\,\mathrm{K})$ is obtained when extrapolating the linear H_a-dependence of the single domain regime back to $H_a = 0$. When plotting the resulting parameters for various temperatures it is possible to fit their temperature dependencies to simple functional forms. The functional form of the spontaneous magnetization $M_\uparrow(T)$ is theoretically well motivated and can be fitted by a power law $M_\uparrow = A(T_C - T)^\beta$. When using A and T_C as fit parameters while keeping the critical exponent β fixed at the 3D Heisenberg value $\beta = 0.38$ one obtains $A = 0.218 \pm 0.0035 \frac{\mathrm{MA}}{\mathrm{mK}^{0.38}}$ and the critical temperature $T_C = 291.89 \pm 0.23$ K very close to the reported literature value [1]. Similarly one can fit $H_c(T)$ to an empirical power law $H_C = H_{max}(T_C - T)^q$. When leaving T_C fixed at $T_C = 291.89$ K one obtains $H_{max} = 0.115 \pm 0.0013 \frac{\mathrm{MA}}{\mathrm{m}}$ and $q = 0.2455 \pm 0.0013$. The peculiar magnetic properties of Gd, likely associated with the field-driven unwinding of a long-period sinusoidal spin structure [11], make it difficult to physically motivate a simple functional form of the magnetic susceptibility below T_C. Here a power law is not an appropriate approximation. To overcome this problem we investigate $\frac{\partial M}{\partial H_a}$ vs T and utilize equation (3) to express $\frac{\partial M}{\partial H_a}$ as $\frac{\partial M}{\partial H_a} = \chi(T) + \frac{M_\uparrow(T)}{H_c(T)}$. With $\frac{M_\uparrow(T)}{H_c(T)} = \frac{\mathrm{A}}{\mathrm{H_{max}}}(T_C - T)^{\beta - q}$ and known parameters A, H_{max}, T_C, β and q we find through a least squares fit that $\chi(T) = \mathrm{X}_0 + \mathrm{X}_1 T + \mathrm{X}_2 T^2$ with $\mathrm{X}_0 = 78.17 \pm 2.3$, $\mathrm{X}_1 = -0.577\,48 \pm 0.016\mathrm{K}^{-1}$, and $\mathrm{X}_2 = 0.001\,07 \pm 2.9 \times 10^{-5}\mathrm{K}^{-2}$ is a good approximating empirical function for $\chi(T)$ for temperature between 280 and 285 K.

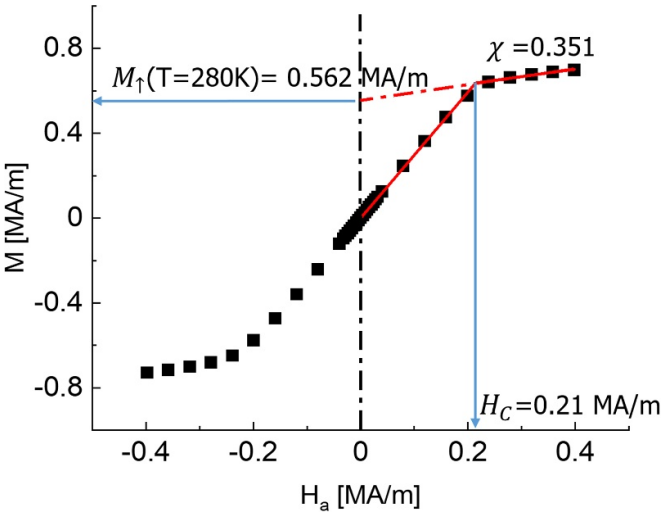

Figure 3. Solid squares show the M vs H_a isotherm of Gd at $T = 280$ K with H_a applied along the easy axis. The data provide the parameters which enter equation (3). Vertical arrow indicates$H_c(T = 280\ \mathrm{K})$. $\chi(T = 280\ \mathrm{K})$ is given by the slope of the linear behavior at $H_a > H_c$. Extrapolation of the linear regime to $H_a = 0$ (dash-dotted line) provides $M_\uparrow(T = 280\,\mathrm{K})$.

2.3. Magnetic field dependence of the heat capacity

Before we model the measured heat capacity, C_{H_a} vs H_a, it is instructive to qualitatively compare heat capacity and magnetization data. Figure 4 shows the corresponding isotherms C_{H_a} vs H_a (squares) and M vs H_a (circles) measured at $T = 280$ K, The heat capacity was measured with the help of a relaxation calorimeter implemented in the Quantum Design Physical Properties Measurement System. The regime of phase coexistence, i.e. up and down magnetization, reveals itself prominently as the demagnetization broadened linear regime in M vs H_a (figure 4 circles). The region is visualized in figure 4 by the two vertical dashed lines at $\pm H_c$. Within the mixed phase region, C_{H_a} vs H_a is virtually constant. This is consistent with the T and H_a-dependence of M in the mixed phase region displayed in figure 2 respectively.

This can be seen when inspecting the expression of the heat capacity change which follows from the Maxwell relation $\left(\frac{\partial s}{\partial H_a}\right)_T = \mu_0\left(\frac{\partial M}{\partial T}\right)_{H_a}$ where $s = S/V$ is the entropy per sample volume. Together with the thermodynamic relation

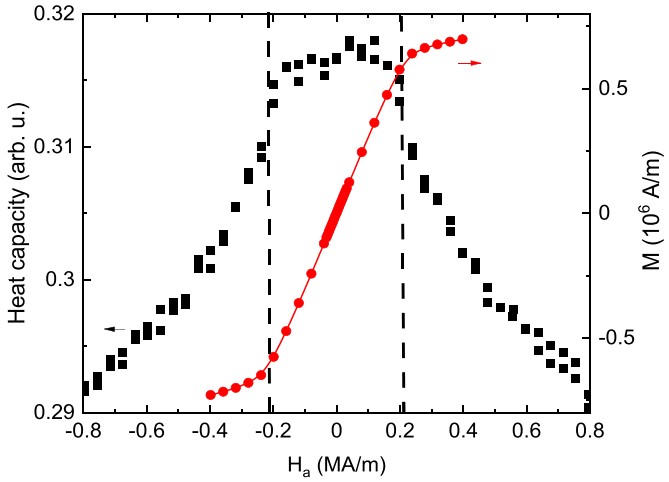

Figure 4. Magnetic field dependence of the heat capacity (squares) measured at $T = 280$ K and magnetization isotherm measured at the same temperature (circles). Field region between the vertical dashed lines indicates the phase coexistence regime of demagnetization broadened first order transition.

$C_{H_a} = T\left(\frac{\partial S}{\partial T}\right)_{H_a}$ one obtains

$$c(H_a, T) - c(H_a = 0, T) = \mu_0 T \int_0^{H_a} \left(\frac{\partial^2 M}{\partial T^2}\right)_{H_a} \mathrm{d}H_a \qquad (4)$$

with $c = C_{H_a}/V$ the volume specific heat capacity. From $c(H_a, T = \text{const}) \approx \text{const}$ follows $\left(\frac{\partial^2 M}{\partial T^2}\right)_{H_a} \approx 0$ which, after two-fold integration, implies $M \approx \tilde{a}(H_a)T + \tilde{b}(H_a)$ with $\tilde{a}(H_a)$ and $\tilde{b}(H_a)$ being temperature independent functions of H_a. Utilizing the experimental finding $M = f(T)H_a$ in the mixed phase region one obtains $M \approx (aT + b)H_a$ with a, b being constants. This approximate result for $M(H_a, T)$ has interesting qualitative consequences we discuss next. First we notice that $\left(\frac{\partial M}{\partial T}\right)_{H_a} = aH_a = \text{const}$ is consistent with the M vs T data shown in figure 2.

Because $\left(\frac{\partial M}{\partial T}\right)_{H_a} \neq 0$ in the mixed phase region there is a nonzero isothermal entropy change

$$\Delta s = s(H_a, T) - s(H_a = 0, T) = \mu_0 \int_0^{H_a} \left(\frac{\partial M}{\partial T}\right)_{H_a} \mathrm{d}H_a \qquad (5)$$

where $s = S/V$ is the entropy density. For $a < 0$, as implied by the data in figure 2, equation (5) yields $\Delta s = \frac{1}{2}\mu_0 a H_a^2 < 0$. The decrease in entropy with increasing applied magnetic field is in agreement with the intuitive picture that the fully demagnetized multi-domain state of high entropy at $H_a = 0$ approaches the state of uniform magnetization with reduced entropy at $H_a = H_c$. Note that a sizable entropy change does not necessarily imply field-dependent change in the heat capacity. Only if the entropy change is temperature dependent there is heat capacity change. Similarly, it is worth to mention that T-dependence of the effective demagnetizing factor $D_{\text{eff}} = \frac{1}{\left(\frac{\partial M}{\partial H_a}\right)_T} = \frac{1}{aT+b}$ originates from M vs T not being constant at $T < T_C$. Therefore, a necessary condition for the validity of the concept of a purely geometry dependent demagnetizing factor is $\left(\frac{\partial M}{\partial T}\right)_{H_a} = 0$ for $T < T_C$. This condition is neither strictly fulfilled for the Gd sample under investigation nor generally strictly observed for other ferromagnets even if their shape is ellipsoidal. Geometries that produce a uniform internal magnetic field under conditions of homogeneous magnetization do not necessarily imply that magnetization remains homogeneous at magnetic fields below saturation. With the help of equations (3) and (4) we obtain a functional form for C_{H_a} vs H_a and apply it to data measured at $T = 280$ K and at $T = 285$ K. Using the density of Gd, $\rho_{\text{Gd}} = 7.9\ \text{g cm}^{-3}$, we convert the volume specific heat capacity change of equation (4) into a mass specific heat capacity change, $\Delta C^{\text{M}} = \frac{\Delta c}{\rho}$. This conversion allows for comparison with the absolute values of the heat capacity measured via relaxation calorimetry in units J gK^{-1}

Figure 5 shows the relaxation calorimetrically measured C_{H_a} vs H_a data (symbols) for $T = 280$ K (squares) and $T = 285$ K (circles) together with single parameter best fits (lines) of functional forms derived with the help of equation (3) and (4). In the case of the $T = 280$ K data (squares) the parameter X_2 was opened as free fitting parameter to obtain a virtually perfect fit in the entire field regime. The fit provides $X_2 = 2.49 \times 10^{-4} \pm 1.6 \times 10^{-5}\text{K}^{-2}$. The need to introduce X_2 as fitting parameter arises because 280 K represents the lower temperature boundary of the measured M vs T data set (see figure 2). Since the M vs T data define the functional shape of $\chi(T)$, the empirical expression for $\chi(T)$ is anticipated to become less trustworthy as temperatures approach 280 K. At $T = 285$ K, nearing the critical temperature, the critical exponent β needed to be treated as a free parameter to achieve a reasonable best fit. The need to adjust β may arise because, nearing T_C, the non-zero magnetic anisotropy of Gd begins to induce a transition from 3D Heisenberg to 3D Ising critical behavior. Indeed, the fit changed the value of β from the 3D Heisenberg value $\beta = 0.38$ used in the magnetic equation of state to $\beta = 0.32 \pm 0.004$ a value close to the 3D Ising critical exponent theoretically predicted to be $\beta = 5/16$ [20]. Crossover from Heisenberg to Ising behavior and the lack of a clear cut distinction between Heisenberg and Ising criticality have been frequently reported for experiments on Gd. It reflects the competition between isotropic exchange favoring Heisenberg interaction and the hexagonal structure of Gd favoring uniaxial magnetic anisotropy with Ising criticality [21, 22].

2.4. Isothermal entropy change and adiabatic temperature change

The data in figure 2 unambiguously show $\left(\frac{\partial M}{\partial T}\right)_{H_a} \neq 0$ for $T < T_C$ giving rise to isothermal entropy change, Δs, in the demagnetization broadened coexistence regime. Δs can be evaluated with the help of equation (5) and utilization of the equation

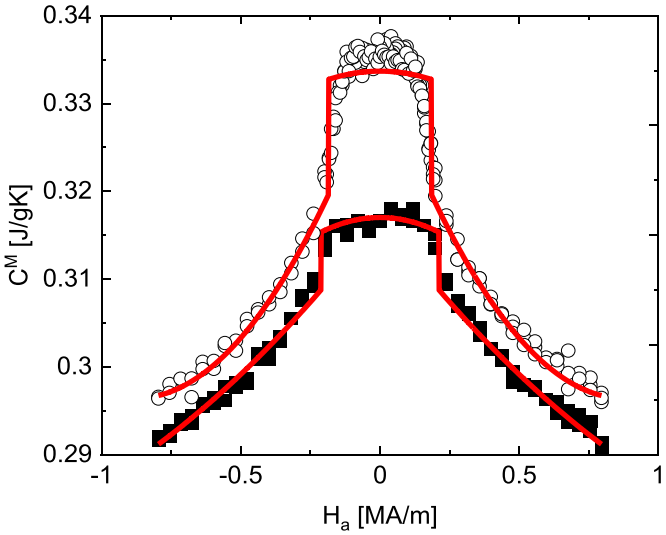

Figure 5. Magnetic field dependence of the heat capacity measured via relaxation calorimetry at $T = 280$ K (squares) and $T = 285$ K (circles). Lines display single parameter best fits (see text).

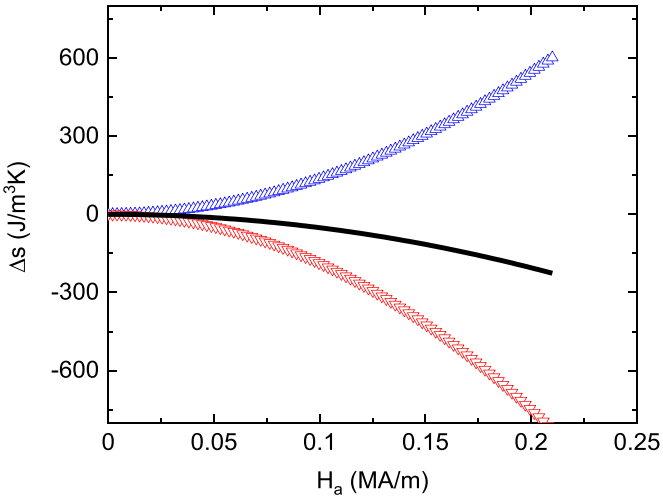

Figure 6. Line shows the magnetic field dependence of the isothermal entropy change, $\Delta s = \Delta s_\chi + \Delta s_{M_\uparrow}$, of Gd at $T = 280$ K calculated from magnetization data with the help of equations (3) and (5). Up (down) triangles show Δs_χ ($\Delta s_{M_\uparrow}$) vs H_a.

of state given by equation (3). Figure 6 show the resulting field dependence of the total isothermal entropy change, $\Delta s = \Delta s_\chi + \Delta S_{M_\uparrow}$ (line), and its decomposition into the two terms $\Delta s_\chi = \frac{\mu_0}{2} H_a^2 \frac{\partial \chi}{\partial T}$ (up triangles) and $\Delta s_{M_\uparrow} = \frac{\mu_0}{2} H_a^2 \frac{\partial}{\partial T}\left(\frac{M_\uparrow}{H_c}\right)$ (down triangles). Δs_χ is the entropy contribution originating from the field-induced magnetization change associated with the local susceptibility $\chi(T)$. Note that Δs_χ increases with increasing H_a contrary to the behavior at $T > T_C$. At $T > T_C$, i.e. in the paramagnetic phase, an applied magnetic field aligns the otherwise disordered spins and thus reduces the entropy. To intuitively understand the behavior at $T < T_C$ one can visualize a virtually uniformly magnetized system where the spontaneous magnetization points downward. At finite temperature $T < T_C$ there are fluctuations which reduce the negative saturation. $\frac{\partial \chi}{\partial T} > 0$ implies that those fluctuations increase on approaching T_C from below just as fluctuations increase on approaching T_C from above. Application of a positive magnetic field will support those fluctuations which oppose the long range order and thus increase entropy.

$\Delta s_{M_\uparrow}$ is associated with the field-induced transition from the demagnetized multi-domain state to the single domain state. Both the spontaneous magnetization $M_\uparrow$ and H_c decrease with increasing temperature. Because $\beta = 0.38 > q = 0.2455$ one finds $\frac{M_\uparrow}{H_c} \propto (T_C - T)^{0.1345}$ and thus $\frac{\partial}{\partial T}\left(\frac{M_\uparrow}{H_c}\right) < 0$ such that $\Delta s_{M_\uparrow}$ decreases with increasing H_a in accordance with the intuitive expectation for the transition from a multi-domain to a single domain state.

Next we utilize the total entropy change Δs to evaluate the adiabatic temperature change, ΔT_{ad}, when increasing the applied field from $H_a = 0$ to $H_a = H_C$. Using $\Delta T_{ad} = -\mu_0 V \int_0^{H_C} \frac{T}{C_{H_a}} \left(\frac{\partial M}{\partial T}\right)_{H_a} dH_a$, the fact that the heat capacity C_{H_a} is virtually constant within the mixed phase region (see figure 6), and $|\Delta T_{ad}| \ll T$ one obtains in very good approximation $\Delta T_{ad} \approx -\frac{T \Delta S}{C_{H_a}}$. At $T = 280$ K and with $H_c = 0.21$ MA m^{-1} we find, $\Delta s = -226.25$ J m^{-3}K^{-1} (see figure 6) and $c_{H_a} = 0.32 \frac{J}{gK} \hat{=} 2.53 \times 10^6$ J m^{-3}K^{-1} (see figure 6) which yields $\Delta T_{ad} = 0.025$ K. Note that, although the adiabatic temperature change in the coexistence regime is small compared to ΔT_{ad} slightly above T_C where magnetocaloric applications take place, it is significant that ΔT_{ad} is non-zero. The insight is that there is an adiabatic temperature change associated with the first order transition which can be missed when artificially correcting the experimental data with the help of an effective demagnetizing factor.

The significance of the demagnetizing field for the magnetocaloric effect has been acknowledged and investigated at $T > T_C$ where magnetization is homogeneous and the concept of a purely geometry dependent demagnetizing factor is applicable. For instance, in [23] the difference in the internal magnetic field associated with the orientation of an applied magnetic field relative to the normal of a plate of Gd has been utilized for magnetocaloric cooling.

2.5. Inference of nanoscale magnetic domains from entropy of the multi-domain state

2.5.1. A simple model to estimate entropy change associated with domain reversal. Given the well-established occurrence of 3D domain branching in uniaxial ferromagnets, we anticipate the presence of small-scale magnetic structures in the demagnetized state of Gd [24–27]. We utilize the field-induced entropy change to estimate the previously unresolved characteristic length scales associated with domain formation in the demagnetized state of Gd. As of today, domains in the basal plane of a Gd bulk single crystal have only been resolved down to micron-sized structures, which are accessible via optical microscopy [28, 29]. It is well-known that domain images limited by optical resolution, such as those obtained via Faraday microscopy in $(LuBi)_3Fe_5O_{12}$, can hide a rich magnetic fine structure. In the case of $(LuBi)_3Fe_5O_{12}$ this fine structure has

been resolved with the help of magnetic force microscopy revealing a striking difference between images obtained with magneto-optical techniques and those which overcome the limitations due to diffraction in the far field [30]. Such high resolution data are, however, not available for the (0001) surface of bulk Gd. Recently, a nanometric spin-stripe periodicity has been experimentally revealed with the help of coherent soft x-ray scattering in an amorphous and centrosymmetric Fe/Gd magnetic thin film [31]. More closely associated with bulk Gd, spin-polarized scanning tunneling microscopy data measured at $T = 5$ K expose branching domains with a periodicity of 160 nm in a 600 atomic layer thick Gd(0001) film on W(110) [32]. For a thin film sample of 120 atomic layers of Gd(0001) on W(110), Härtl *et al* revealed, the presence of stable magnetic structures as small as $\frac{\lambda}{2} = 30$ nm [32]. The authors mentioned that even smaller magnetic structures could not be excluded. Although these interesting findings are not directly transferable to bulk Gd at temperatures of $T = 280$ K, they strongly motivate the search for nanoscale magnetic structures in bulk Gd. The subsequent entropy considerations further support the case for the existence of such nanoscale magnetic structures.

Our entropy approach is based on the assumptions that there is a vast configuration space of nearly degenerate domain structures and that the contribution of the domain wall energy to the total energy of the domain state in the presence of an applied field is small. Although the latter approximation breaks down near $H_a = 0$, it is conceivable to hold for most of the non-zero applied magnetic fields within the mixed phase region. We start by considering the potential energy of a magnetic up/down domain of characteristic volume V_0 in an applied magnetic field. It reads

$$E_{\uparrow,\downarrow} = -\mu_0 \left(\frac{1}{2}\chi(T) H_a + M_{\uparrow,\downarrow}(T) \right) H_a V_0. \tag{6}$$

In the lowest order approximation, the total energy of the domain state is the sum of the potential energies of the individual domains, each with an average volume V_0 approximating the distribution of cluster sizes in a real sample. This crude but useful approximation, allows to evaluate the magnetic field dependence of the entropy of the domain state in terms a two level system [33]

$$S(H_a) = nk_B \left[-f \ln f - (1-f) \ln (1-f) \right] \tag{7}$$

where $n = n_\uparrow + n_\downarrow$ is the total number of domains at $H_a = 0$ and $f = \frac{n_\uparrow}{n_\uparrow + n_\downarrow}$ is the fraction of domains pointing up relative to the orientation of the applied magnetic field. With $V_{\uparrow,\downarrow}/\mathrm{V} = \frac{1}{2}\left(1 \pm \frac{H_a}{H_c}\right)$, $V_{\uparrow,\downarrow} = n_{\uparrow,\downarrow} V_0$, and $V = nV_0$ one obtains

$$\frac{S(H_a)}{V} = \frac{n}{V} k_B \left[-\frac{1}{2}\left(\frac{H_a}{H_c} + 1\right) \ln \frac{1}{2}\left(\frac{H_a}{H_c} + 1\right) - \frac{1}{2}\left(1 - \frac{H_a}{H_c}\right) \ln \frac{1}{2}\left(1 - \frac{H_a}{H_c}\right) \right]. \tag{8}$$

Figure 7 displays $\frac{S(H_a)}{nk_B}$ in accordance with equation (8) (solid line) and its quadratic low field approximation, $\frac{S(H_a)}{\mathrm{nk_B}} \approx \ln 2 - \frac{1}{2}\frac{H_a^2}{H_c^2}$, (dashed line) which is reminiscent of the entropy of Ising spins in a field [34]. Equating $s(H_a) - s(0) \approx -\frac{\mathrm{n}}{\mathrm{V}}\frac{k_B}{2}\frac{H_a^2}{H_c^2}$ with the entropy change $\Delta s_{M_\uparrow} = \frac{\mu_0}{2} H_a^2 \frac{\partial}{\partial T}\left(\frac{M_\uparrow}{H_c}\right)$, allows determining the average volume $V_0 = \frac{V}{n}$ of a characteristic magnetic structure in the demagnetized state as

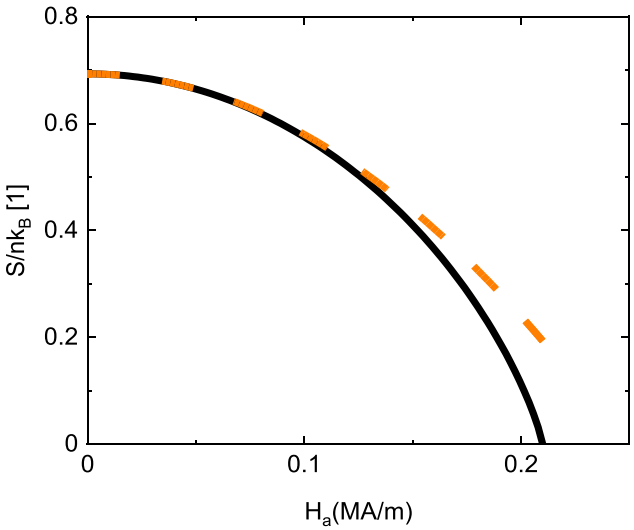

Figure 7. Graphic representation of equation (8) for $H_c = 0.21$ MA m^{-1} (solid line) and its second order Taylor expansion around $H_a = 0$ (dashed line).

$$V_0 = -\frac{k_B}{\mu_0 H_c^2 \frac{\partial}{\partial T}\left(\frac{M_\uparrow}{H_c}\right)} \tag{9}$$

With $\frac{\partial}{\partial T}\left(\frac{M_\uparrow}{H_c}\right) = -\frac{A(\beta - q)}{H_{max}}(T_C - T)^{\beta - q - 1}$ and the numerical values for $A, \beta, q, T_C, H_{max}$ at $T = 280$ K we obtain $V_0 = 8.33 \times 10^{-27}$ m^3. This characteristic magnetic volume corresponds to a characteristic magnetic length $L_0 = V_0^{\frac{1}{3}} \approx 2$ nm. As it is the case in $(LuBi)_3Fe_5O_{12}$, such a small magnetic structure might be the fine structure of branching domains and part of a larger meander domain which is stable against thermal fluctuations.

The experimental observation of a magnetic fine structure in $(LuBi)_3Fe_5O_{12}$ and Gd films makes the above entropy based estimate of hitherto undetected nanoscale magnetic structures in the demagnetized state of bulk Gd plausible. In the absence of a direct experimental observation of such nanoscale magnetic structure in bulk Gd and at $T \gg 5$ K we perform Monte Carlo simulations to test if the simple analytic approach utilizing the entropy of a two level system provides meaningful estimates of magnetic structure sizes.

2.5.2. Relation between cluster size distribution and entropy in the demagnetized state from Monte Carlo simulations. Because Gd is a soft uniaxial ferromagnet with a crossover from Heisenberg to Ising behavior near T_C, the most realistic simulation of the magnetic behavior of Gd at temperatures around $T = 280$ K would utilize an anisotropic 3D Heisenberg model which includes dipolar interaction. The

dipolar interaction is essential to capture the effect of broadening of the isothermal first order transition due to demagnetization effects. The combination of isotropic Heisenberg symmetry and long-range dipolar interaction with open boundary conditions make a 3D simulation computational expensive. To limit the complexity of the problem while still capturing the essential properties we are interested in -specifically, the relationship between magnetic cluster size distribution and entropy- we employ a 3D Ising model with truncated dipolar interaction and a geometry reminiscent of the Gd cylinder of the real sample. A Metropolis algorithm is implemented in a Wolfram Mathematica environment executing 10^5 Monte-Carlo steps for each field or temperature step for a system of $N = N_x \times N_y \times N_z$ spins with $N_x = N_y = 100$ and $N_z = 10$. The classical Ising spins with values $s_i = \pm 1$ point up or down relative to the applied magnetic field oriented along the z-axis. The spins are located on a cubic 3D lattice. Each spin interacts with its respective $z = 6$ nearest neighbors via interaction $J > 0$. We include truncated dipolar interaction with nearest and next nearest neighbors. For a given distance between spins, the dipolar interaction strength is set via the parameter μ which controls the magnetic dipole moment per spin. The Hamiltonian, $\mathcal{H}$, of this cubic 3D Ising system with truncated dipolar interaction reads [35]

$$\mathcal{H} = -J\sum_{\langle i,j\rangle} s_i s_j - H_a \sum_i s_i + \mu \sum_{i\neq j} \frac{s_i s_j}{r_{ij}^3}\left(1 - 3\cos\theta_{ij}\right), \quad (10)$$

where $r_{ij} = |\underline{r}_{ij}|$ is the distance between two spins on sites i and j and θ_{ij} is the angle between the vector $\underline{r}_{ij}$and the z-axis. For $\underline{r}_{ij}$ parallel to the z-axis one finds $\cos\theta_{ij} = 1$ and for $\underline{r}_{ij}$ perpendicular to the z-axis one finds $\cos\theta_{ij} = 0$. The summation over $\langle i,j\rangle$ includes all pairs of neighboring spins and the $i \neq j$-summation is truncated to include nearest and next nearest neighbors. This truncation does not reflect the true long range nature of dipolar interaction but is sufficient to incorporate the desired effects on the hysteresis loops which, for proper choice of μ, eliminates hysteresis and allows to apply equilibrium thermodynamics in the mixed phase region.

Dipolar interaction leads to the formation of magnetic domains. The details of the domain structure are also sensitive to the geometry of the sample. We therefore use open boundary conditions to include the effects of sample geometry and demagnetizing fields created by surface magnetic dipoles. The strength of the dipolar interaction also affects the degree of hysteresis in isothermal loops at $T < T_C$ and the extent of demagnetization at zero applied field. To closely mimic the experimental observation of a fully demagnetized state at $H_a = 0$ in the bulk Gd sample, we adjust the dipolar interaction strength such that hysteresis is minimized to virtually zero. Note that in order to suppress hysteresis in the 3D Ising ferromagnet with truncated dipolar interaction, an unrealistically strong dipolar interaction is required. The very large and truncated dipolar interaction together with the use of an Ising model instead of an anisotropic Heisenberg model, combined with simulating a cubic lattice structure rather than a hexagonal one, implies that the model is not appropriate for simulating Gd. However, the model is well-suited to demonstrate that magnetic cluster sizes can be deduced from an entropy analysis.

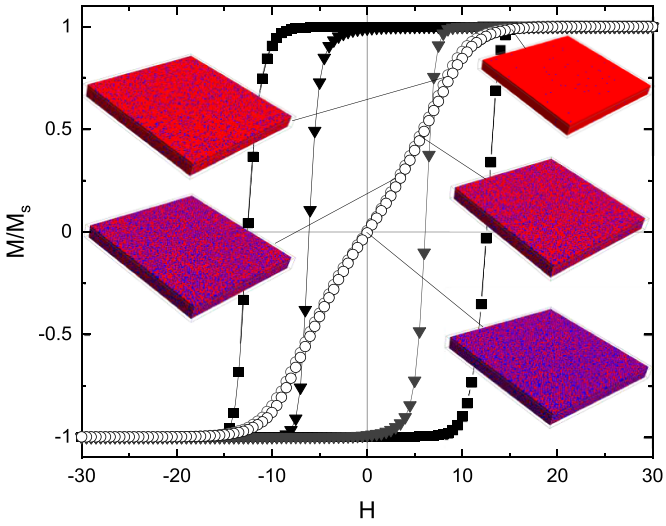

Figure 8. Simulated hysteresis loops for $\mu = 0$ (squares), $\mu = 1.00$ (triangles) and $\mu = 1.61$ (open circles). Images show domain structure at various fields of the down branch of the loop for $\mu = 1.61$.

In a cubic 3D Ising model with $z = 6$ nearest neighbors interacting via ferromagnetic exchange, J, and in the absence of dipolar interaction, the $T = 0$ coercive field reads $H_C^0 = 2zJ$ with $H_C^0 = 12$ for $J = 1$ and $z = 6$. Its Curie temperature is $T_C \approx 4.51 J/k_B$ which, in units with $k_B = 1$ and for $J = 1$, reads $T_C \approx 4.51$. This value is significantly below the mean-field value $T_C \approx \frac{zJ}{k_B}$ known to overestimate T_C. Figure 8 shows isothermal hysteresis loops simulated at $T = 4$ and $J = 1$ for various parameters of dipolar strength $\mu = 0$ (squares), 1.00 (triangles), and 1.61 (open circles). For $\mu = 0$ the simulation reveals a pronounced hysteresis with a coercive field approximately given by $H_C^0 = 12$. With increasing μ the hysteresis decreases until it is virtually suppressed for $\mu = 1.61$. For such a hysteresis-free loop, equilibrium thermodynamics can be applied similar to the experimental data obtained from the Gd sample.

Figure 9 shows the temperature dependence of the magnetization, M, for $\mu = 1.20$ simulated on field-cooling in applied magnetic fields $H_a = 0.5$ (solid line), 0.4 (dashed line), 0.3 (dotted line), 0.2 (dash dot line), and 0.1 (dash dot dot line). The right axis is associated with the simulated magnetization obtained on field-cooling in $H_a = 2$ for strong dipolar interaction with $\mu = 1.61$ (circles). The vertical line marks $T_C \approx 4.51$. The data for M vs T simulated with $\mu = 1.61$ show that with the onset of ferromagnetic long range correlation the magnetization decreases with decreasing temperature. This at first glance unexpected behavior is a consequence of magnetic domain formation where up and down magnetized domains compensate giving rise to a net reduced total magnetization. In

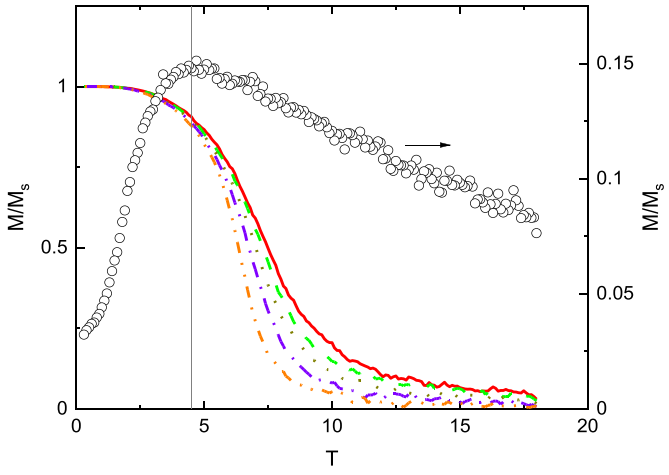

Figure 9. Temperature dependence of normalized magnetization simulated for $\mu = 1.20$ and various applied magnetic fields H_a =0.5 (solid line), 0.4 (dashed line), 0.3 (dotted line), 0.2 (dash dot line), and 0.1 (dash dot dot line) applied during field-cooling. Open circles show T-dependence of normalized magnetization simulated for $\mu = 1.61$ and field-cooling in H_a =2.

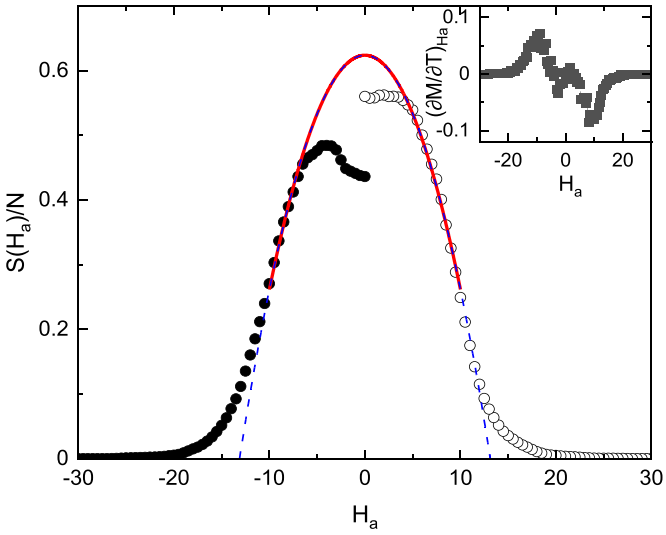

Figure 10. Circles show calculated field dependence of the entropy per spin at $T = 4$. Solid line parabola is the result of a best fit of the S/N vs. H_a using data from the field intervals $-10 \leq H_a \leq -6.5$ and $6.5 \leq H_a \leq 10$. Dashed parabola is an extrapolation outside the fitting regime. The inset shows the numerically calculated $\left(\frac{\partial M}{\partial T}\right)_{H_a}$ vs. H_a.

$H_a = 0$ this compensation is virtually complete in accordance with the zero moment multi domain state of the $\mu = 1.61$ hysteresis (see circles figure 8). For H_a =2, up and down domains do not fully compensate and small field-induced net magnetization remains down to $T = 0$. The low magnetization in the M vs T data below T_C aligns with the narrowing of the hysteresis loops near $H_a = 0$, showing virtually zero remanent magnetization, as observed in the simulation data and in the experimental magnetization isotherms of Gd.

In order to calculate the isothermal entropy change at $T =$ 4 in analogy to the analysis of the experimental isotherms of Gd, we simulate isothermal loops at $T = 4$ and $T = 4.2$ K and numerically approximate the partial T-derivative of M by $\left(\frac{\partial M}{\partial T}\right)_{H_a} \approx \frac{M(T=4.2,H_a)-M(T=4,H_a)}{0.2}$. $\Delta S/N$ is calculated in accordance with equation (5) through numerical integration of $\left(\frac{\partial M}{\partial T}\right)_{H_a}$ with respect to H_a. Because there is very small hysteresis remaining in the simulated loops, we calculate $\left(\frac{\partial M}{\partial T}\right)_{H_a}$ and the entropy change for one of the branches of the loop selected here to be the down branch.

The inset of figure 10 shows $\left(\frac{\partial M}{\partial T}\right)_{H_a}$ vs H_a at $T = 4$ which, after numerical integration and taking into account $S(H_a = 30) \approx 0$, yields S/N vs H_a (circles in main panel of figure 10). S/N vs H_a is calculated separately for data between $-30 \leq H_a \leq 0$ (solid circles) and $0 \leq H_a \leq 30$ (open circles). There is a striking similarity between the data in figure 10 and those shown in figure 7. The simulation data in figure 10 reveal the presence of an intermediate field range where S/N vs H_a follows the quadratic H_a-dependence anticipated by the low field expansion of equation (8). As expected, this simple parabolic behavior breaks down near $H_a = 0$ and smears out with an asymptotic approach of $S = 0$ in the limit of large magnetic fields. The solid line in figure 10 shows a best fit of the functional form $\frac{S}{N} = \alpha H_a^2 + B$ to the S/N vs H_a data within the field regimes $-10 \leq H_a \leq -6.5$ and $6.5 \leq H_a \leq 10$. The dashed parabola extrapolates the fit to outside this regime. The result of the best fit provides the parameters $\alpha = -0.0036 \pm 1 \times 10^{-4}$ and $B = 0.624 \pm 0.009$. Note that $B < \ln 2 \approx 0.7$ implies that, in the fully demagnetized state, the presence of small clusters of uniformly aligned spins is expected rather than random orientation of individual spins. Next we will explore the cluster size distribution in the demagnetized state. The cluster size distribution of up magnetized clusters is utilized to calculate a typical/average cluster size and compare it with the cluster size obtained from the entropy analysis. The validity of the approach used to predict the presence of nanometer-sized magnetic structures in Gd is determined by comparing the two results.

The quadratic approximation of equation (8) implies $(S(H_a) - S(0))/N \approx -\frac{n}{N}\frac{1}{2}\frac{H_a^2}{H_c^2}$ which allows to estimate $\frac{n}{N}$, the number n of average size magnetic clusters per total number of spins N, as

$$\frac{n}{N} = -2\alpha H_C^2. \tag{11}$$

H_C can be defined via the field-coordinate of the inflection point where the isotherm at $T = 4$ K changes its curvature into the convex regime of saturation. This approach yields $H_C = 9$. Substitution of H_C and α into equation (11) yields $\frac{n}{N} \approx 0.58$. That implies that the number of spins which constitute an average size cluster is about 1.7 in qualitative agreement with the

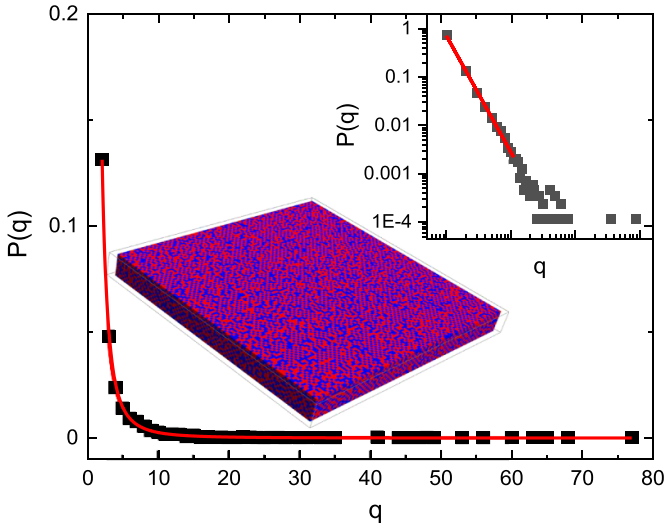

Figure 11. Cluster size distribution (squares) P versus q with P being the relative frequency of finding clusters of up spins forming connected groups of size q. Line is a best fit of a power law $P \propto q^{-s}$ with $s = 2.44$. Inset show the same distribution in a log–log plot together with a linear best fit (line) of slope s.

fine grained magnetic structure displayed in figure 8 for the demagnetized state.

The Monte Carlo simulation allows to determine the cluster size distribution in the demagnetized state. Figure 11 shows the magnetic cluster size distribution of the hysteresis-free $T = 4$ isotherm at $H_a = 0$ (squares). The distribution follows the expected power law behavior $P(q) \propto q^{-s}$ with q being the number of spins within a cluster and s being a temperature dependent exponent which has been reported to vary between 2.2 and 2.5 in the absence of dipolar interaction [36]. The line shows a best fit of this power law behavior which yields $s = 2.44 \pm 0.01$. The depicted domain image shows the fully demagnetized state at $T = 4$ K identical to the one displayed in figure 8. The inset of figure 11 shows the corresponding log–log plot of the cluster size distribution with a linear region of slope s determined by a linear best fit (line). The slope of the linear line is identical to s obtained from the direct fit of the power-law. The log–log data in the inset reveal finite size effects for large clusters through scatter and deviation from the linear behavior. For the subsequent analysis aiming at determining a typical cluster size we therefore employ the result $P(q) \propto q^{-2.44}$ of the fit rather than the noisy data. With the help of $P(q)$ we calculate an average cluster size according to $\langle q \rangle = \frac{\int_1^\infty q^{1-s} \mathrm{d}q}{\int_1^\infty q^{-s} \mathrm{d}q} = \frac{s-1}{s-2}$ which yields $\langle q \rangle = 3.27$ for $s = 2.44$.

Because the power-law distribution is highly skewed, the median, q_{median}, is generally considered to be a better approximation for a typical cluster size than the average $\langle q \rangle$. We therefore calculate q_{median} from the condition $\frac{\int_1^{q_{\mathrm{median}}} q^{-s} \mathrm{d}q}{\int_1^\infty q^{-s} \mathrm{d}q} = \frac{1}{2}$. It yields $q_{\mathrm{median}} = 2^{\frac{1}{s-1}}$. With $s = 2.44$ we obtain $q_{\mathrm{median}} = 1.62$. This value is remarkably close to the typical cluster size estimated via the entropy analysis above which resulted in 1.7 spins in a typical cluster. Correspondingly, we calculate the number of typical clusters per total number of spins according to $\frac{n}{N} = \frac{1}{q_{\mathrm{median}}} = 0.62$ which is very close to the value of $\frac{n}{N}$ estimated via $\frac{n}{N} \approx -2\alpha H_C^2 \approx 0.58$. The fact that these two values agree within less than 7% error is strong evidence that the entropy approach is a meaningful way for the inference of nanoscale magnetic domains in Gd.

3. Conclusion

Gd, recognized as a uniaxial soft ferromagnet and an archetypical magnetocaloric material, still presents many intriguing characteristics that merit further investigation. Its nearly hysteresis-free magnetization isotherms enable the examination of the demagnetization broadened regime of coexisting up and down magnetization within the context of equilibrium thermodynamics. Our magnetometry and calorimetry data suggest that this mixed-phase regime is characterized by an almost constant heat capacity with a slight quadratic dependence on the magnetic field. The transition from a demagnetized multi-domain state to a state of homogeneous magnetization exhibits isothermal entropy change and a small but non-zero adiabatic temperature change. The isothermal entropy change is employed to draw conclusions on the complexity of the demagnetized zero-field state, leading to the prediction of a nanometric magnetic fine structure, which has yet to be experimentally resolved in bulk Gd. Recent studies of Gd and Fe/Gd films strongly suggest the presence of magnetic nanodomains in bulk Gd. In the absence of experiments resolving nanomagnetic structures in the basal plane of bulk Gd, we conducted 3D Monte Carlo simulations with dipolar interaction and open boundary conditions to validate our entropy-based analysis. The estimated number and size of magnetic clusters, derived from entropy considerations using simulated magnetization data, qualitatively matches the number and size of clusters revealed by the cluster size distribution obtained from the Monte Carlo simulation. Thus the simulations robustly supports our conclusion about the presence of nanoscale magnetic structures in bulk Gd, drawn from experimental magnetization data through entropy analysis. We hope this work encourages advanced experimental investigations of the domain structure in the basal plane of bulk Gd and other soft ferromagnets, with the aim of uncovering a potentially rich nanoscale magnetic fine structure that has remained unresolved until now.

Data availability statement

All data that support the findings of this study are included within the article (and any supplementary files).

Acknowledgment

This work is supported by the National Science Foundation/EPSCoR RII Track-1: Emergent Quantum Materials and Technologies (EQUATE), Award OIA-2044049

and by the UNL Grand Challenges catalyst award entitled Quantum Approaches addressing Global Threats. The research was performed in part in the Nebraska Nanoscale Facility: National Nanotechnology Coordinated Infrastructure and the Nebraska Center for Materials and Nanoscience, supported by the National Science Foundation under Award ECCS: 2025298, and the Nebraska Research Initiative.

ORCID iDs

Christian Binek https://orcid.org/0000-0002-0026-0772
Balamurugan Balasubramanian https://orcid.org/0000-0001-6136-3778

References

[1] Dan'kov S Y, Tishin A M, Pecharsky V K and Gschneidner K A 1998 Magnetic phase transitions and the magnetothermal properties of gadolinium *Phys. Rev.* B **57** 3478–90
[2] Gschneidner K A and Pecharsky V K 2000 Magnetocaloric materials *Annu. Rev. Mater. Res.* **30** 387–429
[3] Julia L 2017 Magnetocaloric materials for energy efficient cooling *J. Phys. D: Appl. Phys.* **50** 053002
[4] Franco V, Blázquez J S, Ingale B and Conde A 2012 The magnetocaloric effect and magnetic refrigeration near room temperature: materials and models *Annu. Rev. Mater. Res.* **42** 305–42
[5] Franco V, Blázquez J S, Ipus J J, Law J Y, Moreno-Ramírez L M and Conde A 2018 Magnetocaloric effect: from materials research to refrigeration devices *Prog. Mater. Sci.* **93** 112–232
[6] Frietsch B, Bowlan J, Carley R, Teichmann M, Wienholdt S, Hinzke D, Nowak U, Carva K, Oppeneer P M and Weinelt M 2015 Disparate ultrafast dynamics of itinerant and localized magnetic moments in gadolinium metal *Nat. Commun.* **6** 8262
[7] Simons D S and Salamon M B 1974 Specific heat and resistivity of gadolinium near the Curie point in external magnetic fields *Phys. Rev.* B **10** 4680–6
[8] Pyykkö P 2015 Magically magnetic gadolinium *Nat. Chem.* **7** 680
[9] Oroszlány L, Deák A, Simon E, Khmelevskyi S and Szunyogh L 2015 Magnetism of gadolinium: a first-principles perspective *Phys. Rev. Lett.* **115** 096402
[10] Söderlind P, Turchi P E A, Landa A and Lordi V 2014 Ground-state properties of rare-earth metals: an evaluation of density-functional theory *J. Phys.: Condens. Matter* **26** 416001
[11] Coey J M D, Skumryev V and Gallagher K 1999 Is gadolinium really ferromagnetic? *Nature* **401** 35–36
[12] Franco V, Conde A, Romero-Enrique J M, Spichkin Y I, Zverev V I and Tishin A M 2009 Field dependence of the adiabatic temperature change in second order phase transition materials: application to Gd *J. Appl. Phys.* **106** 103911
[13] Aliev A M, Batdalov A B, Khanov L N, Kamantsev A P, Koledov V V, Mashirov A V, Shavrov V G, Grechishkin R M, Kaul A R and Sampath V 2016 Reversible magnetocaloric effect in materials with first order phase transitions in cyclic magnetic fields: $fe_{48}Rh_{52}$ and $Sm_{0.6}Sr_{0.4}MnO_3$ *Appl. Phys. Lett.* **109** 202407
[14] Liu J, Gottschall T, Skokov K P, Moore J D and Gutfleisch O 2012 Giant magnetocaloric effect driven by structural transitions *Nat. Mater.* **11** 620–6
[15] Mukherjee T, Sahoo S, Skomski R, Sellmyer D J and Binek C 2009 Magnetocaloric properties of Co/Cr superlattices *Phys. Rev.* B **79** 144406
[16] Kivelson S A, Jiang J M and Chang J 2024 *Statistical Mechanics of Phases and Phase Transitions* (Princeton University Press)
[17] Osborn J A 1945 Demagnetizing factors of the general ellipsoid *Phys. Rev.* **67** 351–7
[18] Shah S Q A, Balasubramanian B and Binek C *TMS 2024 153rd Annual Meeting & Exhibition Supplemental Proc.* (Springer) pp 457–65
[19] Hartmann O, Wäppling R, Karlsson E, Kalvius G M, Asch L, Litterst F J, Aggarwal K, Münch K H, Gygax F N and Schenck A 1991 Anisotropic magnetic properties of gadolinium *Hyperfine Interact.* **64** 369–72
[20] Arnold C S and Pappas D P 2000 Gd(0001): a semi-infinite three-dimensional Heisenberg ferromagnet with ordinary surface transition *Phys. Rev. Lett.* **85** 5202–5
[21] Collins G S, Chowdhury A R and Hohenemser C 1986 Observation of isotropic critical spin fluctuations in Gd *Phys. Rev.* B **33** 4747–51
[22] Molho P and Porteseil J L 1983 Magnetic hysteresis near the Curie temperature of Gd *J. Magn. Magn. Mater.* **31–34** 1023–4
[23] Badosa Q, Mañosa L, Vives E, Planes A, Weise B, Beyer L and Stern-Taulats E 2023 Demagnetizing field-induced magnetocaloric effect in Gd *J. Appl. Phys.* **134** 113902
[24] Choksi R, Kohn R V and Otto F 1999 Domain branching in uniaxial ferromagnets: a scaling law for the minimum energy *Commun. Math. Phys.* **201** 61–79
[25] Otto F and Viehmann T 2010 Domain branching in uniaxial ferromagnets: asymptotic behavior of the energy *Calc. Var. Partial Differ. Equ.* **38** 135–81
[26] Minyukov S A and García N 2000 Domain branching in uniaxial ferromagnets under external field *J. Magn. Magn. Mater.* **214** 327–31
[27] Kaczer J 1964 On the domain structure of uniaxial ferromagnets *Sov. Phys.—JETP* **19** 1204–8 (available at: www.jetp.ras.ru/cgi-bin/dn/e_019_05_1204.pdf)
[28] Smith R L, Corner W D and Tanner B K 1980 The magnetic domain structure of gadolinium between 230 and 293 K *J. Magn. Magn. Mater.* **20** 265–70
[29] Smith R L 1978 *Magnetic Anisotropy and Domain Structure in Gadolinium* (Durham University)
[30] Temiryazev A G, Tikhomirova M P and Fedorov I 2003 Surface domains in inhomogeneous yttrium iron garnet films *J. Magn. Magn. Mater.* **258–259** 580–2
[31] Singh A, Li J, Montoya S A, Morley S, Fischer P, Kevan S D, Fullerton E E, Yao DX, Datta T and Roy S 2024 Periodicity staircase in a centrosymmetric Fe/Gd magnetic thin film system *npj Quantum Mater.* **9** 2
[32] Härtl P, Leisegang M and Bode M 2022 Magnetic domain structure of epitaxial Gd films grown on W(110) *Phys. Rev.* B **105** 174431
[33] Hardy R J and Binek C 2014 *Thermodynamics and Statistical Mechanics: An Integrated Approach* (Wiley)
[34] Skomski R, Binek C, Mukherjee T, Sahoo S and Sellmyer D J 2008 Temperature- and field-induced entropy changes in nanomagnets *J. Appl. Phys.* **103** 07B329
[35] Nowak U and Hucht A 1994 Monte Carlo simulation of Ising models with dipole interaction *J. Appl. Phys.* **76** 6341–3
[36] Cambier J L and Nauenberg M 1986 Distribution of fractal clusters and scaling in the Ising model *Phys. Rev.* B **34** 8071–9